

# Numerical Analysis of Particle Separation and Flow Characteristic in Non-woven Filter

Shinya Abe<sup>\*1</sup>, Gen Inoue<sup>\*2</sup>, Yosuke Matsukuma<sup>\*2</sup>, Masaki Minemoto<sup>\*2</sup>

<sup>\*1</sup>Graduate School of Engineering, Kyushu University

<sup>\*2</sup>Faculty of Engineering, Kyushu University

(Received November 12, 2010; accepted January 18, 2011)

In order to improve the performance of the non-woven filter used for IGCC process, it is very important to know the particle behavior in the non-woven filter. In this study, numerical simulation method considered the non-uniform structure is newly proposed in order to predict micro-particle behavior in complex structure. As a result, the particle behavior in the non-woven filter was able qualitatively to be figured out and it is found that the particle adhesion behavior and the internal distribution depend on the transfer parameter of structure. Furthermore, we made the filter characteristic map concerned the behavior of particle adhesion.

## 1. Introduction

In recent years, depletion of energy source and environmental problem has grown into serious problems. Coal has comparatively large amount of deposit, and can be stable source of energy. However, coal emits more carbon dioxide per unit heating value during burning than oil or natural gas. Thus, from the viewpoint of preventing global warming, Integrated coal Gasification Combined Cycle (IGCC) which is one of the high efficiency and environmentally-friendly energy systems is expected. In the IGCC process, micro-particles contained high temperature gas was collected to prevent degradation of gas turbine. Though there are various methods of the collection of microscopic particles, from the viewpoint of pressure drop treatment and mechanical strength, the collection with the non-woven filter is effective for a large-scale exhaust gas treatment such as thermal power plant and waste incineration plant. In the collection with the non-woven filter, the filter and other materials can be broken due to increase pressure drop by particle adhesion, so it is essential to brush down the micro-particle, called by "back washing". Therefore, the non-woven filter used in the collection process is required not only collection efficiency but also aeration performance to decrease running cost in the whole system. In addition, considering high efficiency of various combustion engines, high temperature collection is very important. However, the relationship between these characteristics and structure has never been fully understood yet because it has microscopic and complex structure. Therefore, it is difficult to evaluate the relationship directly by only experiment. In this study, to improve filter performance, the flow collection considered the non-woven structure was calculated, and the characteristic of various structures were examined.

## 2. Numerical analysis

### 2.1 Non-woven filter

The characteristic of the non-woven filter used for numerical analysis was obtained by actual non-woven filter. Fig.1 shows image of the actual non-woven filter by microscope. From this image, the fiber diameter ( $d_f$ )

was obtained. In addition, the porosity ( $\varepsilon$ ) was obtained by calculating from filter volume, mass and density. With these data, simulated non-woven filter was made, shown in Fig.2. The simulated non-woven structure was made by arranging the straight fiber randomly and by stacking the fiber in layers<sup>1)</sup>. In this method, it was assumed to be penetration of the fiber and not to be distortion of the fiber.

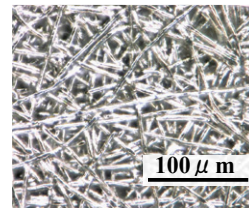


Fig. 1 Actual filter.

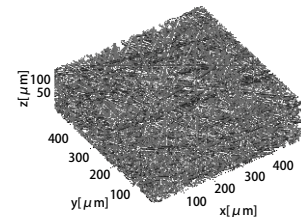


Fig. 2 Simulated filter.

### 2.2 Multi-blocking

In order to calculate the particle concentration distribution with flow, multi-block simulation was developed. First, to use the property data of simulated structure in the flow collection calculation, the simulated non-woven structures were changed the multi-blocking each 10 mesh, and local transfer parameter such as porosity, pore size and permeability were given. Fig.3 is the conceptual diagram of the multi-blocking for simulated non-woven filter. The property data between each block was obtained by the following methods; 1) porosity was given by void ratio of the filter structure, 2) pore size was given by filling virtual sphere in void space, 3) tortuosity was given by using random-walk method that effective transfer length was calculated by moving randomly in void space, 4) permeability was given by approximating adjacent block by single channel. In this way, gas and particle transport in heterogeneous porous structure can be calculated at high speed.

To confirm the validity of simulated non-woven filter, pore size distribution and permeability obtained by the experiment was compared. Fig.4 shows the pore size dis-

tribution of simulated and actual non-woven filter. The pore size distribution of actual filter was obtained by bubble point method. In Fig.4, it was found that two kind of the peak pore size was almost equal. Table 1 shows the permeability obtained by experiment, flow simulation and TS model. The permeability obtained by experiment was calculated by Darcy equation with air flow, thickness pressure drop of through-plane. TS model is the equation of anisotropic permeability in fibrous porous media<sup>2)</sup>. In Table 1, all of these values were almost close. From these results, the validity of this filter structure could be confirmed.

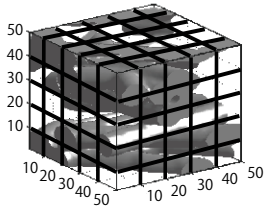


Fig. 3 The concept of multi-block structure.

Table 1 The comparison of permeability (through-plane)

Experiment	$4.612 \times 10^{-13} \text{ m}^2$
Calculation	$4.358 \times 10^{-13} \text{ m}^2$
TS model	$4.210 \times 10^{-13} \text{ m}^2$

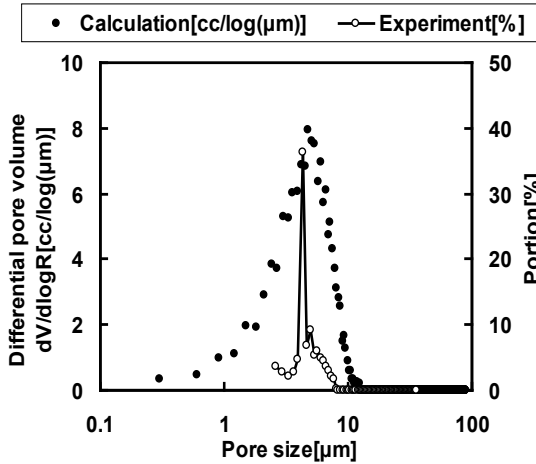


Fig. 4 Pore size distribution.

### 2.3 Filter simulation

In order to calculate the particle transfer, the following equation was used.

$$\frac{\partial \varepsilon C_p}{\partial t} = -v \cdot \nabla (\varepsilon C_p) - m_p A_d S_{eff} \quad (1)$$

where  $C_p$  is the particle concentration,  $\varepsilon$  is the porosity and  $v$  is fluid velocity.  $m_p$  is the particle mass,  $S_{eff}$  is the local effective specific surface area in the non-woven filter and  $A_d$  is the particle attachment coefficient we defined. In this flow simulation, it was assumed that collected particles was dealt with continuum model and calculated as particle concentration transport, and that adhesion rate was a function of only surface area. Fig.5 shows computational system image. The computational system is  $100 \times 100 \times 78$  blocks. The filter size is  $100 \times 100 \times 30$  blocks. Ambient conditions were

assumed as a wall condition. As shown in Fig.5, the gas including the particles inflow from the bottom side. Time step ( $t$ ) is  $1.0 \times 10^{-4}$ s. Particle condition was set as follows; diameter  $0.1 \mu\text{m}$ , volume  $5.24 \times 10^{-22} \text{ m}^3$ , density  $2.26 \times 10^6 \text{ g/m}^3$ . In addition, the inlet particle concentration and the flow rate were set  $0.261 \text{ g/m}^3$  and  $3.35 \times 10^{-9} \text{ m}^3/\text{s}$  respectively<sup>3)</sup>. Though it was necessary to set the value of  $A_d$  by the experiment originally, it was set constant  $1.0 \times 10^{16} \text{ m}^{-2} \text{ s}^{-1}$  in this study.

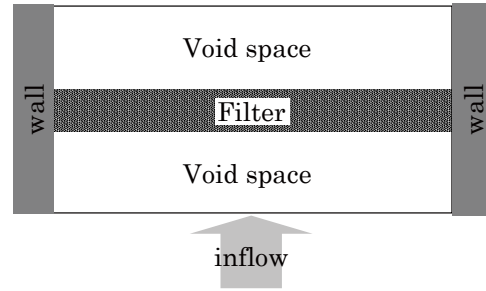


Fig. 5 Computational system image.

### 3. Result

The effect of void structure on the adherent condition was examined. Two kinds of structures with different fiber arrangement were compared with each other. The fiber diameter and the porosity were constant. One has the non-uniform structure (a) and the other has uniform (b), and these figures are shown in Fig.6. In addition, the pore size distribution and the time variation of pressure drop in the two structures are shown as Fig.7 and Fig.8. In Fig.8, dimensionless time  $t_0$  was defined as follows;

$$t_0 = \frac{t}{d/v_z} \quad (2)$$

where  $d$  is the filter thickness and  $v_z$  is average flow rate to direction of filter thickness. From Fig.8, it was found that the pressure drop increased with time because of adhesion and that filter structure affected the variation of pressure drop. Fig. 9 shows the behavior of particle adhesion in the different structures. In Fig.9, (a) is un-uniform filter structure and (b) is uniform filter structure. The filter was set in the area of surrounded by white line. The back gradation shows pressure drop and gray object is the adhesion particles. In this figure, the filter structure was not drawn due to the visualization of adhesion particles and the adhesion particles were drawn as the particle concentration distribution that is not individual particles. In Fig.9, it was confirmed the particle adhered near bottom side of filter at first and that particles trapped at the inside part of filter with time. Particles adhered at the bottom surface of filter as a layer. On the other hand, compared with non-uniform filter, it was found that more particles adhered at the inside of filter in the case of uniform structure in Fig.9 (b). Though the time of particle adhesion is short, it was thought to be due to assume that  $A_d$  is constant. From these results, it was confirmed that the variation of pressure drop and the part of adhesion depended on the filter structure.

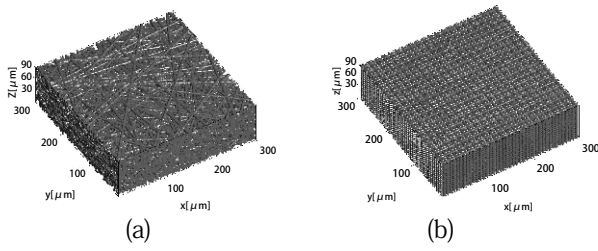


**Fig. 6** Simulated filter ( $\varepsilon$ : 0.4,  $d_f$ : 3.0 $\mu\text{m}$ ).  
(a) : non-uniform structure and (b) : uniform structure

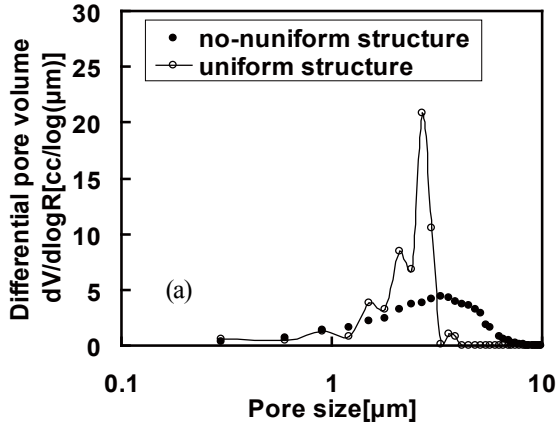


**Fig. 7** Pore size distribution by differential structure.

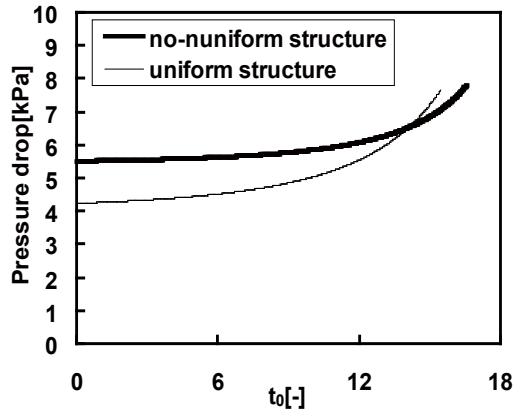


**Fig. 8** The time variation of pressure drop by differential structure.

Next, the influence of structural properties on the distribution of particle adhesion was examined. Fig.10 shows the internal distribution of particle adhesion in the case of each porosity (a) and fiber diameter (b). In this graph, x-axis is the filter thickness and y-axis is the amount of the particle adhesion, and the small value of x-axis shows the bottom side of filter. In Fig.10, the smaller the porosity and the fiber diameter are, the larger the amount of the adhesion on the inflow side is. In other words, particles were caught on the surface of filter. On the other hand, when the porosity and the fiber diameter are large, the particle attachment has happened to the inside. Table 2 shows the pressure drop in each structural condition. In this table, it was confirmed the pressure drop increased as the porosity and the fiber diameter decreased.

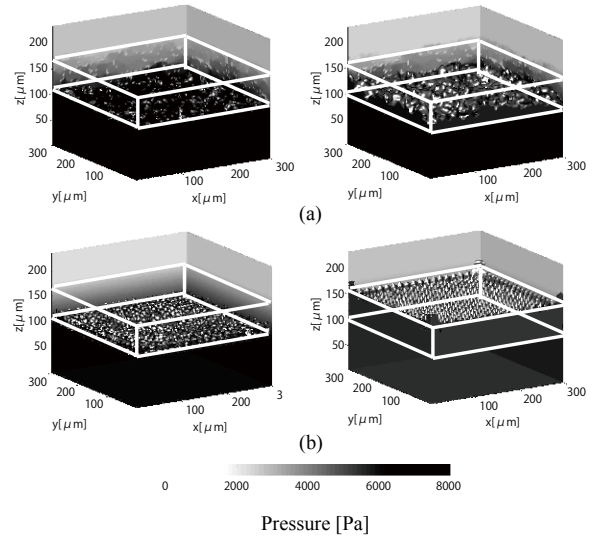


**Fig. 9** Time variation of particle adhesion in  
(a) non-uniform, (b) uniform structure.  
(left:  $t_0=4.2$ , right:  $t_0=8.3$ )

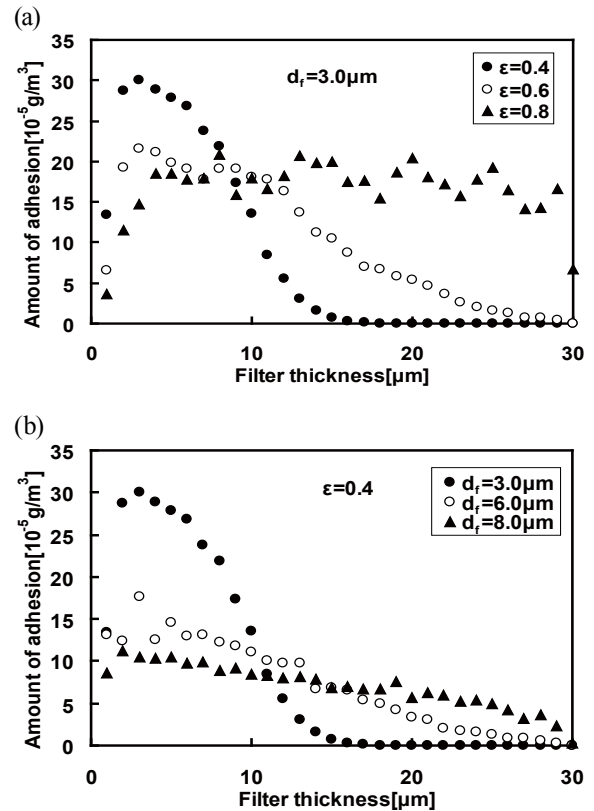


**Fig. 10** Internal distribution of particle adhesion in differences of (a) porosity and (b) fiber diameter ( $t_0=8.3$ ).

**Table 2** Pressure drop in the variable parameters ( $t_0=8.3$ )

$\varepsilon$ [-]	P [Pa]	$d_f$ [ $\mu\text{m}$ ]	P [Pa]
0.4	5300	3.0	5300
0.6	380	4.0	1720
0.8	75	5.0	790

As explained above, the smaller the porosity and the fiber diameter are, the larger the amount of the adhesion on the inflow side is. Furthermore, it is easy to remove adhesion particles from the filter because the particles were collected the surface. However, in this case, it is needed to brush down adhesion particles immediately because the pressure drop was increased rapidly. From these results, we summarized in Fig.11 as filter characteristic map concerning the behavior of particle adhesion. In Fig.11, x-axis is the particle adhesion ratio on surface of filter ( $A_s$ ) and y-axis is the ratio of the time until completely obstructed filter by particle adhesion to the time of standard filter ( $T_p$ ). The data of standard filter is porosity 0.64 and fiber diameter  $3.0\mu\text{m}$ . Then, to improve the filter performance, both value of  $A_s$  and  $T_p$  have to be increased from the viewpoint of the smooth removal of adhesion particles and the decrease of the cycle of back washing. Furthermore, it was found that there is a difference in filter performance by two kinds of structures with different fiber arrangement. In this way, it is necessary to consider the effect of not only overall structural properties such as porosity, fiber diameter and pore size but also heterogeneous structure on filter performance.

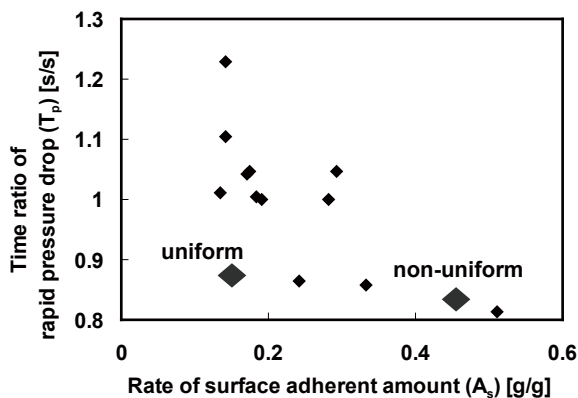


**Fig. 11** Filter characteristic map concerning the behavior of particle adhesion ( $A_s$ : the particle adhesion ratio on surface of filter and  $T_p$ : the ratio of the time until completely obstructed filter by particle adhesion to the time of standard filter).

#### 4. Conclusion

New simulation method was proposed in order to predict micro-particle behavior in the heterogeneous filter structure. The behavior of particle adhesion and the internal distribution could be calculated in each simulated structures. As a result, it is found that the particle adhesion behavior and the internal distribution depend on the transfer parameter of simulated structures. Also, based on the difference of the pressure drop and the ratio of particle adhesion on the surface by structure characteristics, we made the filter characteristic map which can be applied to design the optimal filter. In our future study, we will try to clarify the actual phenomena and to examine various filter structures. Moreover, it will be necessary to compare with experimental value, so we will conduct experiment in the future.

**Acknowledgement:** This research was supported by Grant-in-Aid for Young Scientists (A) of the Ministry of Education, Culture, Sports, Science and Technology. The author (Shinya Abe) is also grateful for the educational program provided by the Global-Center of Excellence in Novel Carbon Resource Sciences, Kyushu University.

#### References

- 1) G. Inoue, T. Yoshimoto, Y. Matsukuma, M. Minemoto, *J Power Source*, **175**, 145 (2008).
- 2) J. T. Gostick and M.W. Fowler, *J Power Source*, **162**, 228 (2006).
- 3) T. Sera, K. Inoue, *Mitsubishi Heavy Industry Technical Report*, **33**(1), 14 (1996).